



Chelation-based iron uptake mitigates the effects of prolonged high-temperature stress in cool-season grasses

Received: 11 October 2024

Accepted: 6 August 2025

Published online: 28 August 2025

 Check for updates

Anzu Minami^{1,2} , Yoshihiko Onda¹, Minami Shimizu¹, Yukiko Uehara-Yamaguchi¹, Asaka Kanatani¹, Risa Nakayama¹, Kyoko Toyama¹, Kotaro Takahagi¹, Komaki Inoue¹, Tomoko Nozoye^{3,4}, Motofumi Suzuki⁵, Yusuke Kouzai¹, Toshihisa Nomura^{1,6}, Keitaro Tanoi^{1,6}, Masaki Endo⁷, Ryuji Miki⁸, Masakazu Kashiwara⁸, Naoaki Taoka⁸ & Keiichi Mochida^{1,2,9} 

High-temperature stress poses a significant threat to agricultural productivity and ecological diversity. Here, we show the effects of prolonged high-temperature stress on wheat (*Triticum aestivum*) and the model grass *Brachypodium distachyon* and demonstrate that heat stress induces iron deficiency in newly emerged leaves. Quantitative trait locus analysis of *B. distachyon* reveals a genomic region associated with heat resilience that includes the transporter of mugineic acid family phytosiderophores 1 gene (*BdTOM1*). Iron-deficiency-related genes including *BdTOM1* are more highly expressed in a high-temperature-tolerant *B. distachyon* accession at high temperature than in a sensitive accession, resulting in greater secretion of deoxymugineic acid. Treatment with proline-2'-deoxymugineic acid mitigates heat-induced growth inhibition, but excess iron treatment leads to toxicity in both species. Our findings highlight the role of heat-induced nutritional stress in prolonged high-temperature stress and suggest that iron homeostasis could provide a promising target for improving crop resilience to climate extremes.

Climate change threatens plant productivity and crop yields, especially for cool-season cereals like wheat (*Triticum aestivum*). These crops are predicted to suffer substantial yield losses due to greater exposure to heat stress during their growth and reproductive periods^{1–5}. Heat stress disrupts critical physiological reactions such as photosynthesis and respiration, leading to lower crop yields^{6–8}. In plant cells, heat stress increases plasma membrane fluidity and impairs electron transport chains in chloroplasts and mitochondria, causing excessive production of reactive oxygen species (ROS), protein misfolding, lipid peroxidation, DNA damage, and disruption of cellular homeostasis^{9–14}. To

mitigate these negative effects, plants sense and respond to heat stress through the heat-shock response, which includes the activation of calcium signaling pathways, the maintenance of membrane integrity, the prevention of cell death, and the transcription of heat shock factor (*HSP*) genes, encoding proteins that regulate the expression of heat shock protein (*HSP*) genes involved in ROS scavenging and possessing molecular chaperone functions^{15–19}.

Experimental designs aimed at exploring the heat-stress response in plants have been primarily based on short-term heat-shock treatments, using exposure to temperatures more than 15 °C above the

¹RIKEN Center for Sustainable Resource Science, Yokohama, Kanagawa, Japan. ²Kihara Institute for Biological Research, Yokohama City University, Yokohama, Kanagawa, Japan. ³Center for Liberal Arts, Meiji Gakuin University, Minato-ku, Tokyo, Japan. ⁴Graduate School of Agricultural and Life Sciences, The University of Tokyo, Bunkyo-ku, Tokyo, Japan. ⁵Aichi Steel Corporation, Tokai, Aichi, Japan. ⁶Faculty of Agriculture, Yamagata University, Tsuruoka, Yamagata, Japan. ⁷Institute of Agrobiological Sciences, National Agriculture and Food Research Organization, Tsukuba, Ibaraki, Japan. ⁸Agri-Bio Research Center, Kaneka Co. Ltd, Iwata, Shizuoka, Japan. ⁹School of Information and Data Sciences, Nagasaki University, Nagasaki, Nagasaki, Japan. ✉e-mail: anzu.minami0@gmail.com; keiichi.mochida@riken.jp

optimum growth temperature^{20–22}. However, climate change results in prolonged heat stress at moderately high temperatures (around 35 °C), causing a sustained shift from growth to stress acclimation, which slows plant development, growth, and reproduction. Understanding plant responses to prolonged moderate heat stress is critical for improving crop resilience to climate change.

Iron is an essential micronutrient with important roles in photosynthesis and respiration. The iron concentration inside plant cells must be tightly regulated in order to avoid both iron overload and iron deficiency^{23–26}. Despite the abundance of iron in the soil, its bioavailability is limited because it predominantly exists as insoluble ferric iron (Fe³⁺). Therefore, graminaceous plants, including rice (*Oryza sativa*), wheat, and *Brachypodium distachyon*, primarily rely on a chelation-based Strategy II mechanism to take up Fe³⁺ from the soil^{27,28}. These plants produce phytosiderophores such as mugineic acids, which are released into the rhizosphere via a Transporter Of Mugineic acid family phytosiderophores (TOM)-like efflux transporter to chelate Fe³⁺^{28,29}. The Fe³⁺–phytosiderophore complexes are then taken up into the cell via iron transporters such as YELLOW STRIPE 1 and YELLOW STRIPE1-LIKE (YSI, YSL) family members^{30–32}. However, whether moderate heat stress impairs iron homeostasis in graminaceous plants is unclear.

In this work, we address this question by focusing on bread wheat and *B. distachyon*, a model species closely related to Triticeae crops and more suitable for genetic analysis due to its smaller genome³³. We explore acclimation mechanisms that enhance resilience to prolonged high-temperature stress in these species and demonstrate a role for Strategy II iron uptake in this process in graminaceous plants. Quantitative trait locus (QTL) analysis of two *B. distachyon* accessions with different heat-stress responses identifies *BdTOM1* as a candidate gene in the heat-stress response. *BdTOM1* is more highly expressed in high-temperature-tolerant accessions under heat conditions, leading to increased 2'-deoxymugineic acid secretion. Treatment with the synthetic mugineic acid analog, proline-2'-deoxymugineic acid (PDMA) mitigates iron deficiency that accompanies heat stress through restoring iron homeostasis. By contrast, excessive iron treatment leads to high levels of ROS accumulation under high temperatures. Our findings highlight the role of iron homeostasis via the Strategy II iron uptake mechanism in enhancing heat-stress tolerance in cool-season grasses like wheat and *B. distachyon*. Furthermore, this study suggests that managing heat-induced nutritional stress may offer a key strategy for enhancing crop resilience to climate change and securing food production in the face of rising global temperatures.

Results

Prolonged exposure to high temperatures is accompanied by iron deficiency in wheat

We explored the consequences of prolonged high-temperature stress on bread wheat, the most widely cultivated cool-season cereal, as it faces significant threats from climate change. Following growth for 2 weeks under high-temperature conditions (HC, 32–35 °C), seedlings from wheat cultivar ‘Fielder’ weighed significantly less than control seedlings grown for 2 weeks under normal-temperature conditions (NC, 22–25 °C), and their emerging leaves were chlorotic (Fig. 1a, b). Simple ratio pigment index (SRPI, Fig. 1c) values for chlorophyll content and photochemical reflectance index (PRI, Fig. 1d) values indicating the photosynthetic output were lower in stressed vs. unstressed leaves. This observation was independently supported by lower F_v/F_m values, representing the maximum potential quantum efficiency of photosystem II (PSII), which were 0.79 ± 0.01 for NC seedlings and 0.69 ± 0.01 for HC seedlings, indicating diminished photosynthetic efficiency (Fig. 1e).

Because various nutrient deficiencies cause growth inhibition and leaf chlorosis³⁴, we conducted ionome analysis to assess the nutrient composition of wheat leaves. Measurements of the major metals in

wheat leaves revealed a 54.5% lower iron (Fe) content and 56% higher magnesium (Mg) and 95% higher manganese (Mn) contents under HC vs. NC (Fig. 1f). The lower Fe content under HC was accompanied by a massive upregulation of *TaIRO2.6*, a homolog of the rice *iron-related basic helix-loop-helix transcription factor 2* (*IRO2*), encoding a key regulator of iron-deficiency-responsive genes involved in iron uptake^{27,35} (Supplementary Fig. 1), suggesting that seedlings exposed to HC also experience Fe deficiency. Indeed, under HC, the leaf color changed from yellow-green to darker green with age, in conjunction with the downregulation of *TaIRO2.6* (Fig. 1g, h). These findings suggest that age-dependent leaf chlorosis presumably results from high-temperature-induced Fe deficiency. Transferring the plants from HC to NC after a 3-week cultivation period fully rescued the leaf chlorosis and alleviated leaf damage, indicating that the observed chlorosis and cessation of growth are reversible responses to high-temperature stress (Supplementary Fig. 2). These findings suggest that prolonged high-temperature stress induces Fe deficiency that leads to lower biomass production in wheat.

High-temperature-induced reductions in biomass vary among in *B. distachyon* accessions

Wheat is a hexaploid species with a large genome and duplicated genes across multiple subgenomes, complicating gene identification. Therefore, we used the genetically related diploid species *B. distachyon* with a smaller genome to explore genes that are involved in the resilience to prolonged high-temperature stress using various genetic techniques³³. Similar to wheat seedlings, *B. distachyon* seedlings exhibited substantial growth inhibition under prolonged high-temperature stress, as evidenced by their shorter stature and lower plant weight compared with those grown under NC (Fig. 2a). However, this response varied among accessions (Supplementary Fig. 3a, Supplementary Data 1). For example, accession Bd21 (sensitive to high temperatures) showed more pronounced symptoms, including lower biomass and marked chlorosis of newly emerged leaves under HC vs. NC, while accession Bd21-3 (tolerant to high temperatures) demonstrated greater HC tolerance in terms of biomass accumulation and leaf greening (Fig. 2a–d). Supplementary Fig. 3b shows weekly measurements of SPRI and PRI values of Bd21 and Bd21-3 grown with non-chelated Fe under NC and HC. SPRI values of both accessions were stable under NC but decreased under HC. The PRI values of Bd21 increased under NC but rapidly decreased under HC. In Bd21-3, the PRI values remained stable under NC and decreased under HC, but to a lesser degree than in Bd21. To assess whether *B. distachyon* seedlings exposed to HC were Fe deficient, we examined the expression levels of *BdIRO2.1*, the counterpart of *TaIRO2.6* and *OsiIRO2* in *B. distachyon* (Supplementary Fig. 1). Indeed, *BdIRO2.1* was upregulated in the leaves of Bd21 and Bd21-3 seedlings grown under HC compared with those grown under NC, suggesting HC-induced Fe deficiency (Fig. 2e). The leaf Fe content of both accessions was lower under HC than under NC, with Bd21-3 leaves containing 61% less Fe under HC compared with those under NC. Notably, the Fe content of Bd21 leaves was 91% lower under HC than that under NC, suggesting that Bd21 is more susceptible to severe Fe depletion under HC than Bd21-3 (Fig. 2f). These findings indicate that HC-induced Fe deficiency occurs in both wheat and *B. distachyon*, suggesting a common vulnerability of cool-season grasses to HC. Importantly, the differing responses of *B. distachyon* accessions points to possible genetic diversity in their resilience to continuous high temperatures.

Based on the observed difference in high-temperature resilience between Bd21 and Bd21-3, we looked for genetic factors underlying this heat-induced growth inhibition. We performed QTL analysis using two F₂ populations derived from the crosses Bd21-3 × Bd21 and Koz4 (tolerant to high temperature) × Bd21 using fresh biomass weight under HC as the phenotype. This analysis identified a major QTL on chromosome 4 (Supplementary Fig. 3c). Examination of a recombinant

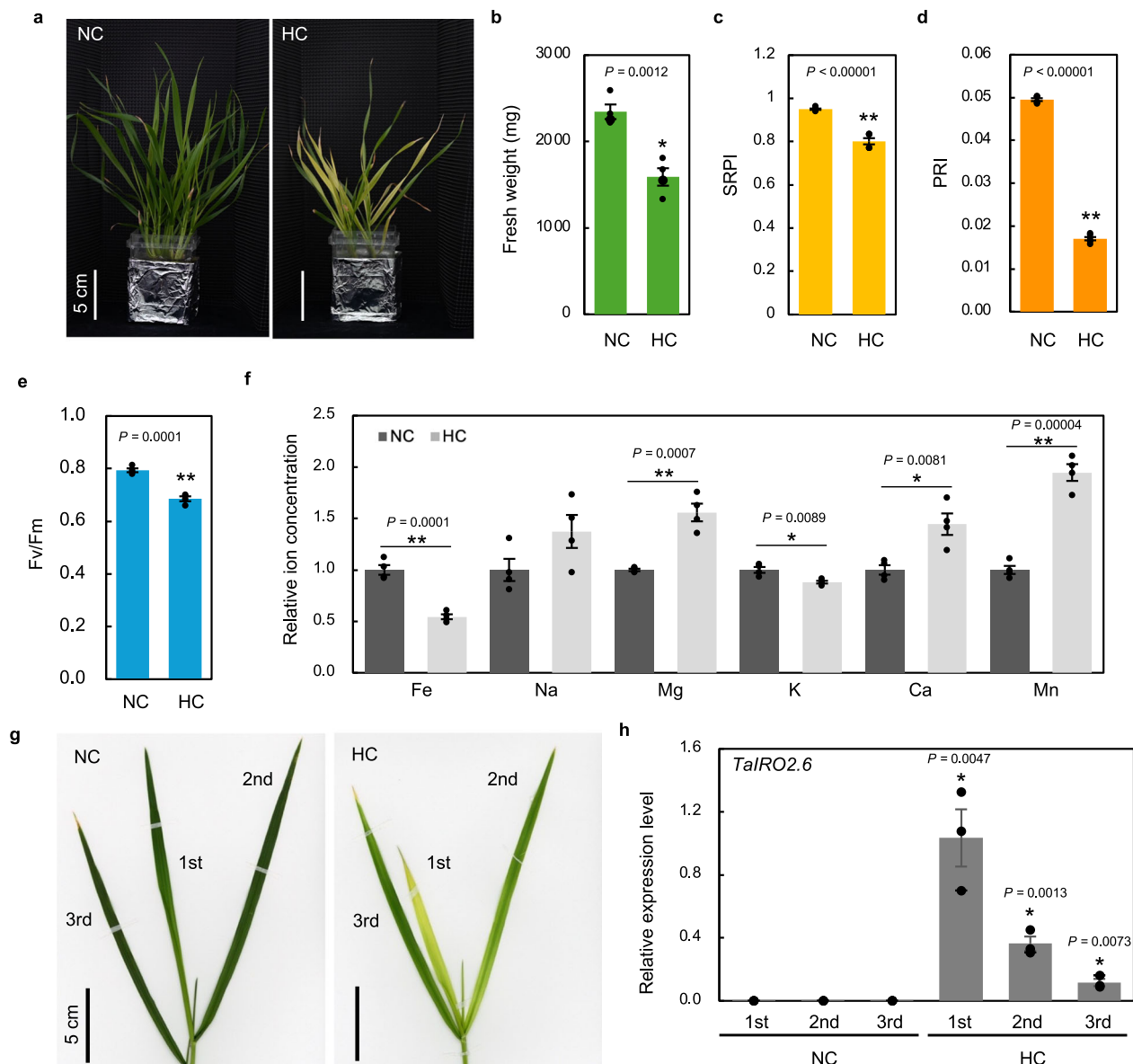


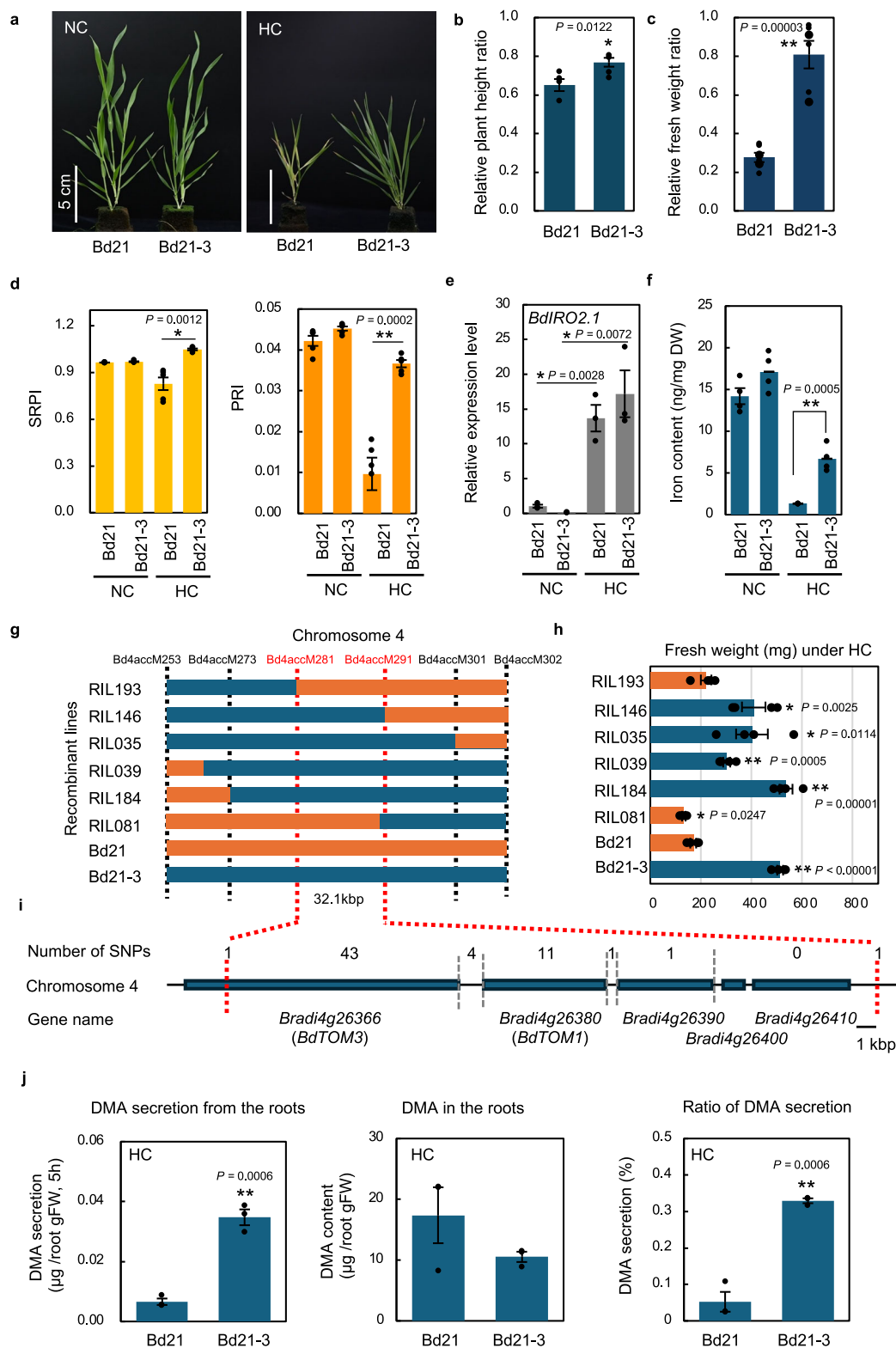
Fig. 1 | Iron deficiency develops in wheat following prolonged exposure to high temperatures. **a** Wheat cultivar ‘Fielder’ grown hydroponically for 2 weeks under normal (NC, 22–25 °C) or high-temperature (HC, 32–35 °C) conditions with non-chelated iron [$\text{Fe}_2(\text{SO}_4)_3$] as the sole iron source. Scale bars, 5 cm. **b** Aboveground fresh weight of wheat plants after 2 weeks of growth under NC or HC. Simple ratio pigment index (SRPI, **c**) and photochemical reflectance index (PRI, **d**) from second fully expanded leaves grown under NC or HC for 2 weeks. **e** Maximum quantum yield (F_v/F_m) from the second fully expanded leaf blade of seedlings grown under NC or HC for 2 weeks. **f** Relative concentrations of the indicated metal elements in

leaf blades from seedlings grown under NC and HC for 2 weeks. **g** Newly emerging leaves of seedlings with or without prolonged high-temperature stress. Seedlings were grown hydroponically with non-chelated iron under NC or HC for 4 weeks. Scale bars, 5 cm. **h** Relative expression of the iron deficiency-marker gene *TaIRO2.6* in the leaves of wheat seedlings grown under NC or HC for 4 weeks. Data are means \pm SEM ($n = 4$ in **(b, e, f)**; $n = 6$ in **(c, d)**; $n = 3$ in **(h)** biological replicates). * $P < 0.05$ and ** $P < 0.001$, from two-tailed Student’s *t* tests between NC and HC; the exact *P* values for significant differences are given in the graphs. Source data are provided as a Source Data file.

inbred line population derived from the F_2 progeny of a Bd21-3 \times Bd21 cross narrowed this QTL peak to a 32.1-kb region containing 62 single nucleotide polymorphisms (SNPs) and five annotated genes (Fig. 2g–i, Supplementary Fig. 3d). This region harbors two tandemly located and highly similar genes, *BdTOM3* (Bradi4g26366) and *BdTOM1* (Bradi4g26380), which are putative homologs of the efflux Transporter Of Mugineic acid (TOM) family of phytosiderophores (Supplementary Fig. 4).

In graminaceous plants, TOM transporters enhance iron uptake by releasing mugineic acids, which chelate and thus help solubilize Fe^{3+} in the rhizosphere (Supplementary Fig. 5). Thus, to investigate whether the difference in heat tolerance between Bd21 and Bd21-3 was related

to mugineic acid secretion, we measured the amounts of mugineic acids within root tissues and released by roots of Bd21 and Bd21-3 seedlings growing under HC (Fig. 2j). After 2 weeks of HC treatment, heat-tolerant Bd21-3 secreted more 2'-deoxymugineic acid (DMA) than heat-sensitive Bd21. More DMA accumulated in Bd21 roots than in Bd21-3 roots, and the DMA secretion rate from root tissues was significantly lower in Bd21 than in Bd21-3. This suggests that Bd21 roots biosynthesize DMA but do not secrete as much DMA as Bd21-3. These results suggest that the amount of DMA secreted from roots is related to the heat tolerance of *B. distachyon* and that greater secretion of DMA by the roots of Bd21-3 seedlings contributes to improved iron uptake, which enhances high-temperature tolerance.



The three remaining genes in the QTL region, *Bradi4g26390*, *Bradi4g26400*, and *Bradi4g26410*, encode a ribosome assembly protein, a calmodulin, and a Ser/Thr kinase, respectively. We did not detect any polymorphisms in the coding sequences of *Bradi4g26400* or *Bradi4g26410*, and there were slight changes in transcript levels in response to HC in either leaves or roots (Fig. 2i, Supplementary Data 2, Supplementary Fig. 6). By contrast, *Bradi4g26390*, a potential

homolog of *Arabidopsis thaliana* *HEAT STRESS TOLERANT DWD 1³⁶*, which negatively regulates heat tolerance, possesses SNPs distinguishing Bd21-type and Bd21-3-type accessions, and its expression responded to HC. Accordingly, we cannot rule out its potential role in heat tolerance. Nevertheless, due to the associated iron deficiency observed under prolonged HC, we concentrated our efforts on the two most relevant genes: *BdTOM1* and *BdTOM3*.

Fig. 2 | QTL mapping of high-temperature stress resilience in *Brachypodium distachyon*. **a** *B. distachyon* accessions Bd21 and Bd21-3 grown under normal (NC) or high-temperature (HC) conditions with non-chelated iron $[\text{Fe}_2(\text{SO}_4)_3]$. Two-leaf stage seedlings grown in artificial phenolic resin block containing 2.5 mg Fe L^{-1} of non-chelated iron for 3 weeks. Scale bars, 5 cm. Relative plant height (**b**) and fresh weight (**c**) of seedlings in (**a**). HC values are normalized to those of NC (HC/NC). $n = 6$, biological replicates. **d** Simple ratio pigment index (SRPI) and photochemical reflectance index (PRI) from the first fully expanded leaves grown under NC or HC for 4 weeks. $n = 5$, biological replicates. **e** Relative expression of the iron deficiency marker gene *BdIRO2.1* in the first fully expanded leaves grown under NC or HC for 4 weeks. $n = 3$, biological replicates. **f** Leaf Fe content of seedlings grown under NC or HC for 4 weeks. $n = 4$, biological replicates. **g** Genotypes of

recombinant inbred lines (RILs) between SNPs Bd4accM253 and Bd4accM302 in Bd21 genome. Single nucleotide polymorphism (SNP) positions are shown at the top with recombinant numbers. Orange: Bd21 fragment; blue: Bd21-3 fragment. **h** Aboveground fresh weights of RILs from a Bd21-3 \times Bd21 cross after 25 days of prolonged high-temperature treatment. $n = 4$, biological replicates. **i** The 32.1-kb candidate region between SNP markers (Bd4accM281 and Bd4accM291). **j** Secretion and root levels of 2'-deoxymugineic acid (DMA) in *B. distachyon* Bd21 and Bd21-3 seedlings grown hydroponically with non-chelated iron under HC for 2 weeks $n = 3$, technical replicates. Data are means \pm SEM. * $P < 0.05$ and ** $P < 0.001$ (two-tailed Student's t tests: between Bd21 and Bd21-3 in (**b–d, g, j**); between NC and HC in (**e**); between Bd21 and RILs in (**h**). Exact P values for significant differences are given in the graphs. Source data are provided as a Source Data file.

BdTOM1 counteracts Fe deficiency in *B. distachyon*

We investigated whether *BdTOM1* and/or *BdTOM3* transcript levels respond to HC or Fe deficiency in *B. distachyon* accessions Bd21 and Bd21-3. *BdTOM1* was gradually upregulated in the roots of seedlings as HC continued, with Bd21-3 showing a significantly greater response than Bd21, whereas *BdTOM3* was primarily expressed in the leaves where it did not respond to HC (Fig. 3a). The transcript levels of the mugineic acid biosynthesis genes *DEOXYMUGINEIC ACID SYNTHASE* (*BdDMAS*), *NICOTIANAMINE AMINOTRANSFERASE 1* (*BdNAAT1*), and *MUGINEIC ACID 3-DIOXYGENASE 3* (*BdIDS3*) and the Fe-deficiency marker gene *BdIRO2.1* also increased in the roots of Bd21-3 and Bd21 in response to heat stress, especially in Bd21-3 (Supplementary Fig. 7a). We also assessed the expression of *BdTOM1* and *BdTOM3* in plants grown in Fe-free solution: *BdTOM1* was significantly upregulated in roots under Fe-free conditions under both NC and HC, with Bd21-3 again exhibiting a more pronounced response (Fig. 3b). Under Fe-free conditions, *BdIRO2.1* was also upregulated, particularly in the roots of Bd21-3 seedlings under HC (Supplementary Fig. 7b). The expression levels of their orthologous genes *TaTOM1*, *TaIRO2.6*, and *TaDMAS* in wheat also rose under HC relative to NC (Supplementary Fig. 7c).

To elucidate the roles of *BdTOM1* and *BdTOM3*, we generated genome-edited mutant lines in the *B. distachyon* Bd21 background (Supplementary Fig. 8) and assessed their phenotypes. The *Bdtom1* mutants exhibited severe growth defects even under NC, whereas the *Bdtom3* mutants showed normal growth under NC (Fig. 3c, d). The Fe contents of leaves from the *Bdtom1* mutants, but not the *Bdtom3* mutants, were significantly lower than those of the wild type (Fig. 3e). We also observed the significant upregulation of *BdIRO2.1* in the roots of *Bdtom1* but not *Bdtom3* mutants compared with levels in the wild type (Fig. 3f), suggesting that Fe deficiency specifically occurred in the *Bdtom1* mutants. Additionally, the introduction of a complementation construct constitutively expressing *BdTOM1* into the *Bdtom1* #1 mutant background resulted in healthy plants with downregulated *BdIRO2.1* expression (Supplementary Fig. 9). To investigate whether the Fe deficiency observed in the *Bdtom1* mutants was due to impaired mugineic acid-mediated Fe uptake, we applied the synthetic mugineic acid analog PDMA to seedlings grown hydroponically in the presence of non-chelated Fe in the form of $\text{Fe}_2(\text{SO}_4)_3$. Treatment with PDMA alleviated the severe growth defects of the *Bdtom1* mutants and led to relatively high Fe content across all genotypes (Fig. 3c–e). We also observed this phenotypic rescue of the *Bdtom1* mutants upon PDMA treatment in soil-grown plants (Supplementary Fig. 10). These results indicate that BdTOM1, but not BdTOM3, is involved in mugineic acid-mediated Fe uptake in *B. distachyon* and that BdTOM1, rather than BdTOM3, may function as a phytosiderophore transporter responsive to HC-induced Fe deficiency in the roots of *B. distachyon* plants.

We performed genomic complementation of the *Bdtom1* mutant with genomic fragments containing the *BdTOM1* allele derived from either Bd21 or Bd21-3 (Supplementary Fig. 11). As the recipient line, we used the *Bdtom1* #3 mutant (Bd21-3 background), which carries a single-base G insertion at the same site as the CRISPR-induced A insertion in the *Bdtom1* #4 mutant (Bd21 background). The *Bdtom1* #3

mutants exhibited growth defects even under NC conditions (Supplementary Fig. 12a), consistent with the Bd21-background mutants (Fig. 3c). Transformation with either allele of the *BdTOM1* genomic fragment restored growth under NC, indicating that both alleles can functionally complement the mutation. This phenotypic recovery was also supported by reduced *BdIRO2* expression, suggesting alleviation of iron deficiency (Supplementary Fig. 12b). Under HC, PRI values were significantly reduced in the *Bdtom1* #3 mutant (Supplementary Fig. 12c). In contrast, the Bd21-3-allele-complemented lines maintained PRI values more comparable to those under NC than did the Bd21-allele-complemented lines, suggesting that the Bd21-3 allele may contribute to improved photosynthetic performance during heat stress.

To define the temporal sequence of events leading to Fe deficiency in response to HC, we investigated the expression patterns of *HSF* and *HSP* genes under our experimental conditions. *BdHSF17* and *BdHSP70-2* reached peak expression at 3 or 7 days into HC, which was earlier than the peak for the iron-deficiency marker genes examined, with expression of most genes peaking at 14 days into HC treatment (Supplementary Fig. 7a). The expression levels of *BdHSF17* and *BdHSP70-2* under NC and HC were unaffected by Fe-free treatment (Supplementary Fig. 7b). Unlike *BdIRO2.1*, *BdHSP70-2* expression was comparable among the wild type, *Bdtom1*, and *Bdtom3* deletion lines (Fig. 3f), suggesting that BdTOMs do not regulate *HSP70-2* expression. Therefore, it is likely that the initial response to high-temperature stress by HSFs and HSPs is not influenced by the iron deficiency response.

Variation in *BdTOM1* is cryptic in a *B. distachyon* population

We assessed the possible association of *BdTOM1* haplotypes with plant growth under NC or HC using 153 *B. distachyon* accessions (Supplementary Data 1). We identified accessions carrying SNPs between Bd21 and Bd21-3 in the genomic region encompassing *BdTOM1* and *BdTOM3* based on our whole-genome resequencing data (Supplementary Data 2). For *BdTOM1*, 101 accessions harbored the Bd21-3 sequence and 52 carried the Bd21 sequence (Fig. 4a). When measuring fresh biomass of seedlings growing under NC and HC, we did not observe significant differences among accessions regardless of their *BdTOM1* haplotype under NC. However, under HC, accessions with the Bd21-3 allele exhibited significantly higher fresh biomass than those with the Bd21 allele (Wilcoxon rank-sum U test, P -value = 2.327×10^{-7}). This association between *BdTOM1* haplotypes and resilience against HC-induced growth inhibition in the *B. distachyon* population supports our findings that BdTOM1 mitigates HC-induced Fe deficiency. By contrast, *BdTOM3* showed a different pattern: The Bd21 haplotype of *BdTOM3* was present in 150 of the 153 accessions analyzed, and the Bd21-3 haplotype was present in the three remaining accessions (Supplementary Data 2). Combined with our expression analysis and characterization of genome-edited mutants, these findings suggest that BdTOM3 is unlikely to be involved in the response to HC-induced Fe deficiency.

Additionally, we examined the relationship between the *BdTOM1* haplotype and the geographical distribution of 50 accessions with the Bd21 haplotype and 97 accessions with the Bd21-3 allele collected from

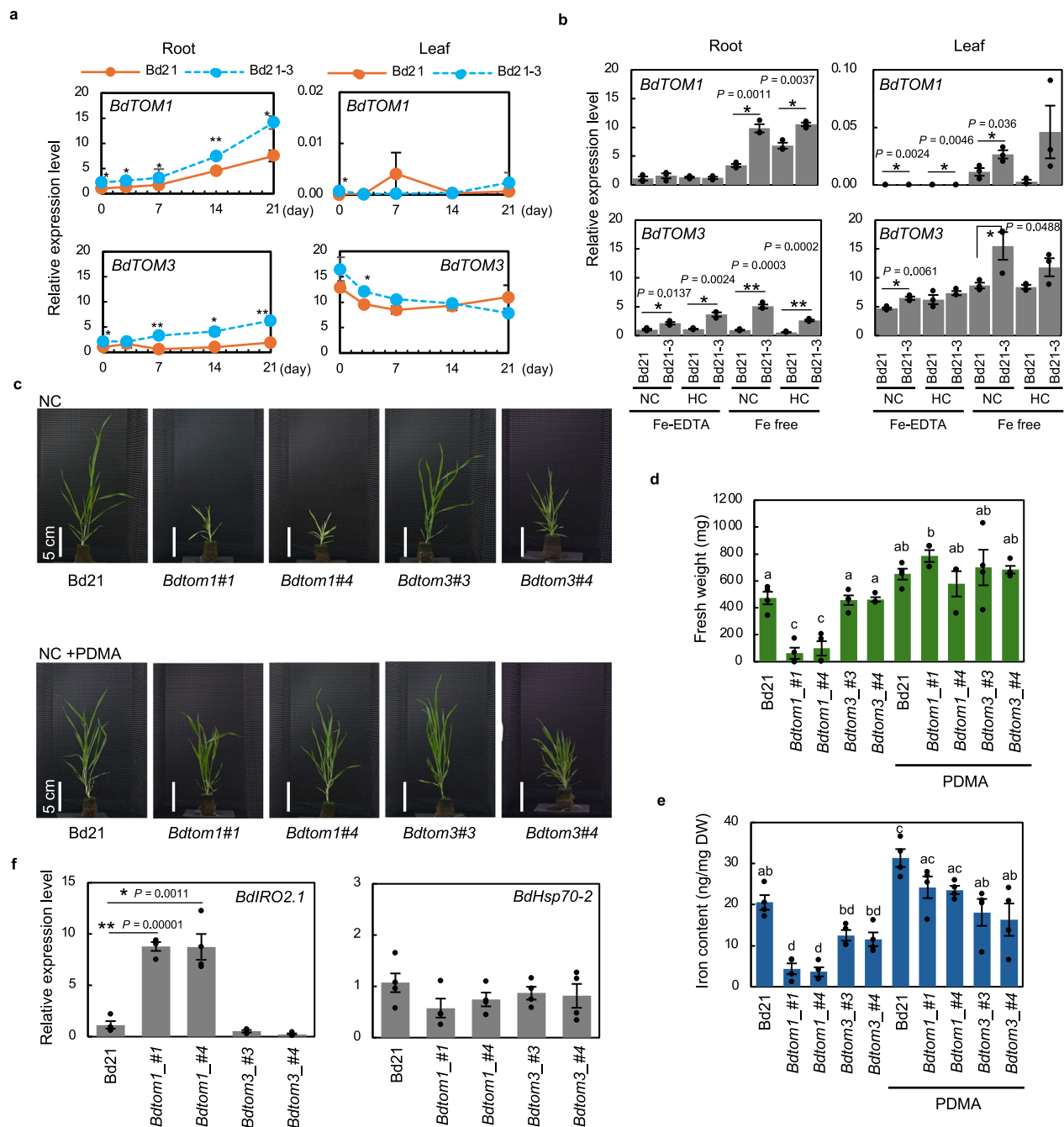


Fig. 3 | *BdTOM1* confers resilience to Fe deficiency in *Brachypodium distachyon*.

a Expression of *BdTOM1* and *BdTOM3* in *Bd21* and *Bd21-3* accessions grown in artificial phenolic resin blocks containing 2.5 mg Fe L⁻¹ of non-chelated iron [Fe₂(SO₄)₃] under HC for 3 weeks. The first fully expanded leaves and root tissues were collected at the indicated time points. **P* < 0.05; ***P* < 0.001 (two-tailed Student's *t* test, *Bd21* vs *Bd21-3*; *n* = 3, biological replicates). **b** *BdTOM1* and *BdTOM3* expression in seedlings grown hydroponically with 2.5 mg Fe L⁻¹ chelated iron (Fe-EDTA) or without iron (Fe-free) under NC or HC for 1 week. **P* < 0.05; ***P* < 0.001 (two-tailed Student's *t* test, *Bd21* vs *Bd21-3*; *n* = 3, biological replicates). **c** *Bd21*, *Bdtom1*, and *Bdtom3* plants grown in artificial phenolic resin blocks containing 2.5 mg Fe L⁻¹ non-chelated iron (NC) alone or with 30 μM proline-2'-deoxymugineic acid (NC + PDMA) under NC for 4 weeks. Aboveground fresh weight (**d**) and leaf Fe

content (**e**) of *Bd21*, *Bdtom1*, and *Bdtom3* plants grown in artificial phenolic resin blocks containing 2.5 mg Fe L⁻¹ non-chelated iron alone or with 30 μM PDMA under NC for 4 weeks. Different lowercase letters indicate significant differences between groups [one-way ANOVA; **d**: *F* (9, 29) = 16.01, *P* = 5.11 × 10⁻⁹, *n* = 3–4; **e**: *F* (9, 30) = 15.68, *P* = 4.41 × 10⁻⁹, *n* = 4; Tukey's HSD test, two-sided, adjusted for multiple comparisons]. **f** Expression of iron deficiency-marker *BdIRO2.1* and heat shock protein *BdHSP70-2* in the roots of *Bd21*, *Bdtom1*, and *Bdtom3* seedlings grown in artificial phenolic resin blocks containing 2.5 mg Fe L⁻¹ non-chelated iron under NC for 4 weeks. **P* < 0.05, ***P* < 0.001 (two-tailed Student's *t* tests, *Bd21* vs. each mutant line; *n* = 4, biological replicates). Data are means ± SEM. Exact *P* values for significant differences are labeled on the graphs. Source data are provided as a Source Data file.

Turkey (Supplementary Data 3). Although we observed a significant difference in their longitudinal distribution (Mann–Whitney *U* test, *P*-value = 2.4e⁻⁰⁶), there was no significant difference in their latitudinal distribution (Mann–Whitney *U* test, *P*-value = 0.042), and the *Bd21*- and

Bd21-3-type alleles did not form distinct regional clusters (Fig. 4b). These findings suggest that these alleles may be cryptic, without distinct phenotypes, under the local climatic conditions of their geographical locations.

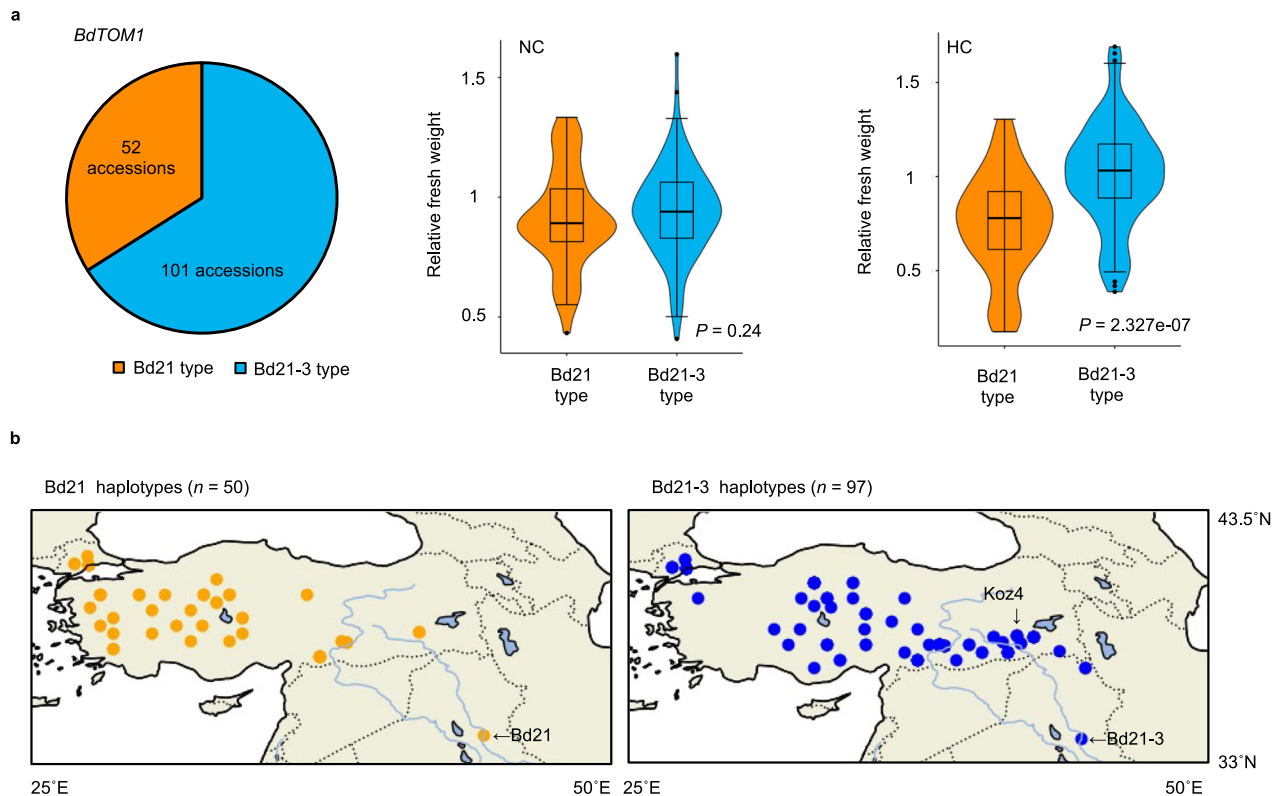


Fig. 4 | *BdTOM1* polymorphisms among *Brachypodium distachyon* accessions.

a Association of nonsynonymous SNP variants in *BdTOM1* with seedling fresh weight for 153 *B. distachyon* accessions grown under NC or HC (Supplementary Data 1). A total of 153 *B. distachyon* accessions were classified into two haplotype groups, Bd21-type ($n = 52$) and Bd21-3-type ($n = 101$), based on their *BdTOM1* genotype (Supplementary Data 2). Orange: Bd21-type; blue: Bd21-3-type. The center lines represent the median, box limits represent the 25th and 75th percentiles, whiskers extend to the minimum and maximum values within 1.5 times the

interquartile range, and the violin shapes show the data distribution density. A Wilcoxon rank-sum *U* test was conducted to evaluate the differences between the two groups. **b** Geographical distribution of *BdTOM1* haplotypes in Turkey. Latitude and longitude for each accession are shown. The Bd21 and Bd21-3 accessions were collected near Salakudin in Iraq. The sampling locations of 50 Bd21-type accessions (orange) and 97 Bd21-3-type accessions (blue) were obtained from previously published data⁷² (Supplementary Data 3). Images show latitudes 33° to 43.5° and longitudes 25° to 50°. Source data are provided as a Source Data file.

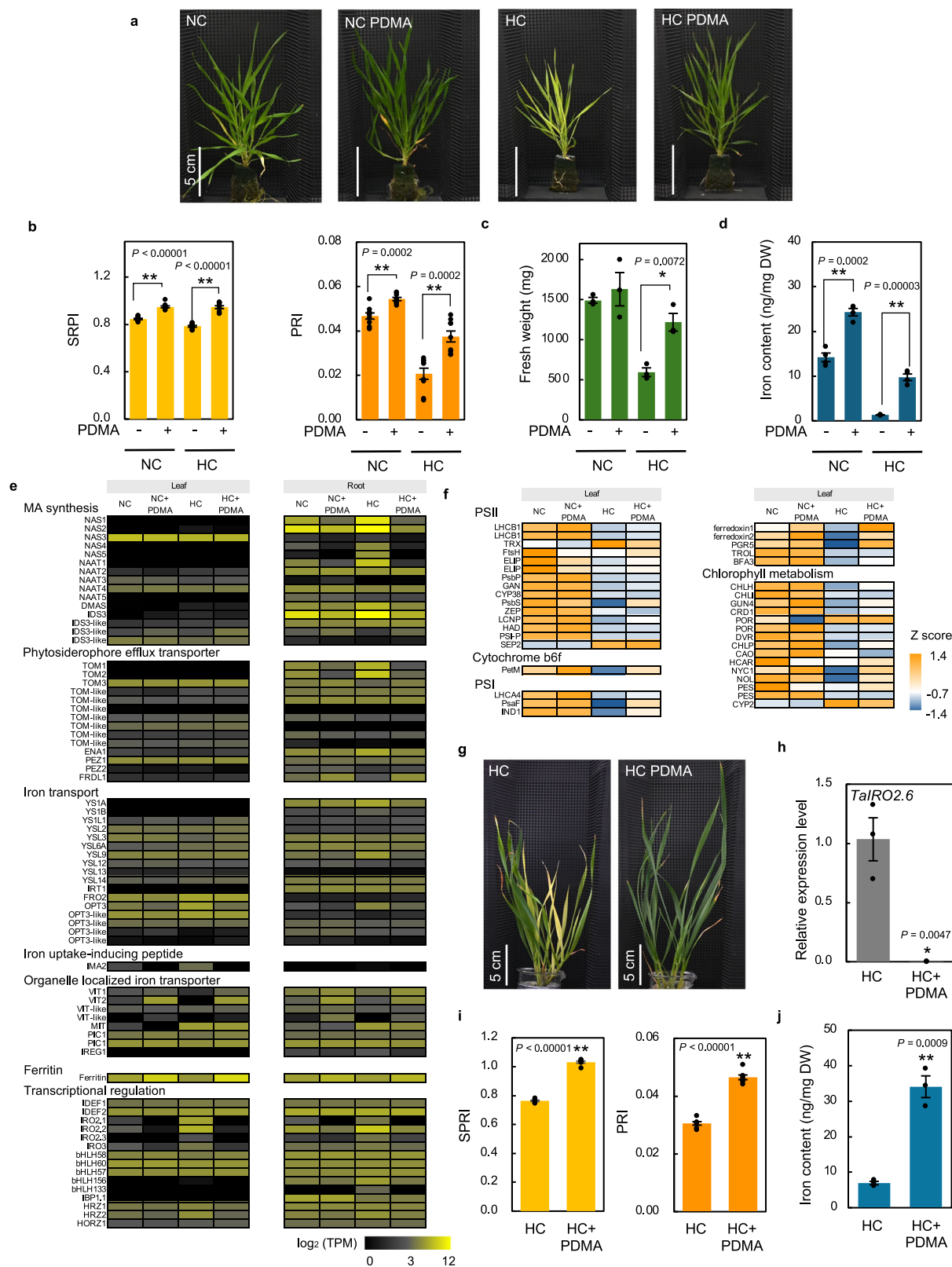
PDMA treatment enhances high-temperature resilience by targeting mugineic acid-mediated Fe uptake in cool-season grasses

To explore the potential of our findings for practical applications in economically significant cereals like wheat, we assessed whether PDMA treatment enhances resilience to high-temperature stress through improved Fe uptake. In the high-temperature-sensitive *B. distachyon* accession Bd21, PDMA treatment significantly improved leaf greening, SPRI and PRI values, fresh biomass, and Fe content in plants grown under prolonged HC (Fig. 5a–d). Transcriptome analysis indicated that PDMA treatment effectively mitigates the transcriptional response to Fe deficiency in roots under HC, lowering the expression of Fe-deficiency-responsive genes involved in Fe chelation, including genes encoding proteins related to mugineic acids biosynthesis, phytosiderophore efflux transporters, Fe-uptake-related transporters, and transcriptional regulators of iron deficiency (Fig. 5e, Supplementary Data 4). Additionally, iron-storage-related genes, such as *Vacuolar iron transporter* (*VIT*) genes and *Ferritin*, were upregulated upon PDMA treatment. Photosynthesis-related and chlorophyll metabolism genes were downregulated in response to HC, but PDMA treatment counteracted the reduced expression of genes involved in PSII, cytochrome *b₆f*, PSI, and chlorophyll metabolism (Fig. 5f, Supplementary Data 5). PDMA treatment improved leaf greening in wheat seedlings and led to lower expression levels for the Fe-deficiency marker gene *TaIRO2.6* and significantly elevated Fe contents under prolonged HC (Fig. 5g–j). These findings suggest that PDMA application effectively enhances resilience to high-temperature stress by supporting Fe homeostasis and photosynthesis, highlighting

its potential as an agent to improve growth and development in cool-season cereals experiencing prolonged heat-stress conditions.

We analyzed the effects of PDMA treatment at concentrations of 3, 30, 150, or 300 μ M on *B. distachyon* Bd21 seedlings grown under HC in the presence of non-chelated Fe (Fig. 6a). At PDMA concentrations as low as 3 μ M, SRPI and PRI values were higher than those without PDMA, indicating improved photosynthetic efficiency; values remained high even at 30 and 150 μ M. At a concentration of 300 μ M, PRI values declined, suggesting that the plants were under stress at high PDMA concentrations (Fig. 6b). The expression levels of the iron-overload-marker gene *BdFerritin*, encoding an Fe-storage protein, also indicated that treatment with high concentrations of PDMA causes iron overload under HC (Fig. 6c). Notably, the chelated Fe form Fe(III)-EDTA was more effective than the non-chelated Fe form $\text{Fe}_2(\text{SO}_4)_3$ in enhancing photosynthetic capacity under HC, as indicated by PRI values. However, the effect of Fe(III)-EDTA in mitigating heat stress was not greater than that of PDMA. We analyzed the dose-dependent effects of PDMA treatment in wheat cultivar ‘Fielder’ (Supplementary Fig. 13a–c). At a low PDMA concentration of 3 μ M, SRPI and PRI values were higher than those without PDMA, while PRI values declined at PDMA concentrations greater than 30 μ M. Furthermore, the effect of PDMA was stronger than that of Fe(III)-EDTA, similar to the results observed in *B. distachyon* Bd21.

We explored HC-dependent Fe overload and oxidative damage by growing Bd21 plants in Fe-excess medium under NC or HC. Under Fe-overload conditions, HC caused more pronounced growth defects and ROS accumulation than NC (Fig. 6d). The expression of *BdFerritin*



increased under both NC and HC, suggesting that Fe overload induces stronger oxidative damage under HC (Fig. 6e). We obtained similar results for Fe-overload experiments under HC in wheat cultivar Fielder (Supplementary Fig. 13d). These findings underscore the importance of a finely tuned Fe-acquisition response for maintaining Fe homeostasis and preventing Fe-induced oxidative damage, particularly under HC, in both the model plant *B. distachyon* and wheat.

Discussion

This study focused on prolonged but moderate heat stress rather than short-term and severe heat-shock treatment, which causes immediate and critical cell damage. Prolonged high-temperature stress imposes cumulative stress on plants, causing them to alter their physiological mechanisms to adapt to high temperatures, ultimately leading to growth inhibition. Here, we demonstrated that maintaining Fe

Fig. 5 | The synthetic deoxymugineic acid proline-2'-deoxymugineic acid enhances plant resilience to high-temperature stress. **a–d** *B. distachyon* Bd21 plants grown in phenolic resin blocks containing 2.5 mg Fe L⁻¹ of non-chelated iron [Fe₂(SO₄)₃] under NC or HC for 4 weeks in the presence (+) or absence (–) of 30 μM proline-2'-deoxymugineic acid (PDMA). **a** Representative images of plants. **b** Simple ratio pigment index (SRPI) and photochemical reflectance index (PRI) values from the first fully expanded leaf. **c** Aboveground fresh weight. **d** Leaf Fe content. *n* = 9, 3, and 4 for (**b–d**), respectively. **e, f** Four-leaf-stage Bd21 seedlings were treated with 2.5 mg Fe L⁻¹ non-chelated iron in the presence or absence of 30 μM PDMA under NC or HC for 1 day. The first fully expanded leaves and root tissues were collected for RNA-seq analysis. **e** Fe deficiency-related gene expression. Each row represents one gene, and colors represent mean expression levels as log₂-normalized TPM values. Lower expression levels are shown in black, and higher expression levels are shown

in yellow. **f** Photosystem and chlorophyll metabolism-related gene expression. Differentially expressed genes in response to high temperature are shown. Each row represents one gene, and colors represent mean expression level as z-score values. A positive z-score (orange) denotes values greater than the mean, and a negative z-score (blue) denotes values below the mean. **g–j** Effect of PDMA treatment on wheat 'Fielder' grown hydroponically with 2.5 mg Fe L⁻¹ of non-chelated iron in the presence (+) or absence (–) of 30 μM PDMA under HC for 4 weeks. **g** Representative images of plants. **h** *TaIRO2.6* expression in the first fully expanded leaves. **i** SRPI and PRI values from the first fully expanded leaf. **j** Leaf Fe content. *n* = 3 for (**h, j**), *n* = 7 for (**i**). Data are means ± SEM. **P* < 0.05 and ***P* < 0.001, from two-tailed Student's *t* tests comparing values with and without PDMA; samples represent biologically independent replicates; exact *P* values for significant differences are shown on each graph. Source data are provided as a Source Data file.

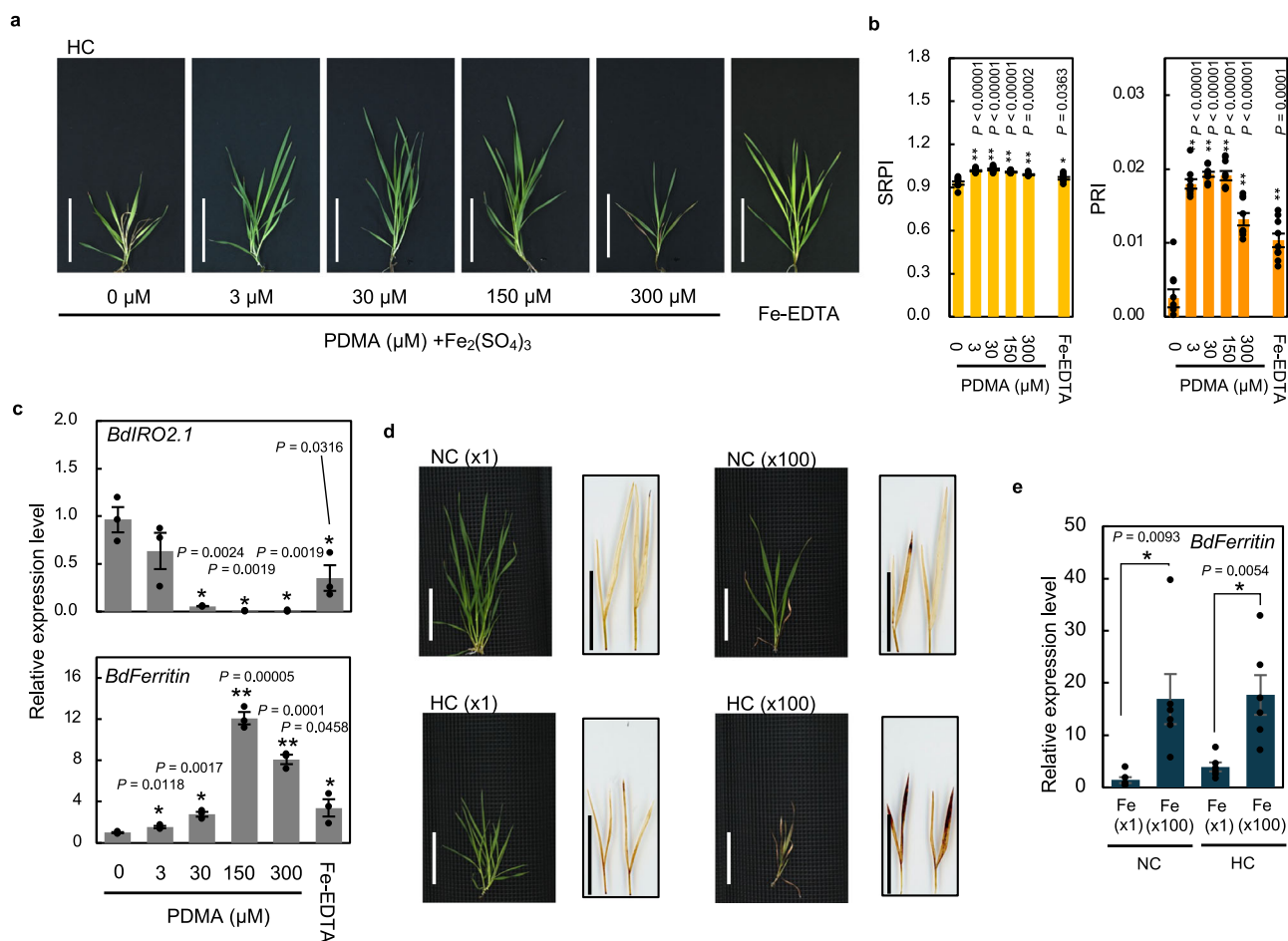


Fig. 6 | Dose-dependent effect of proline-2'-deoxymugineic acid and iron toxicity in *Brachypodium distachyon* under high-temperature conditions. **a** *B. distachyon* Bd21 grown hydroponically with 2.5 mg Fe L⁻¹ non-chelated iron [Fe₂(SO₄)₃] in the absence (–) or presence (+) of proline-2'-deoxymugineic acid (PDMA) at the indicated concentrations under HC for 3 weeks. For chelated iron (Fe-EDTA) treatment, plants were grown with 2.5 mg Fe L⁻¹ of Fe-EDTA under HC for 3 weeks. Scale bars, 5 cm. **b** Simple ratio pigment index (SRPI) and photochemical reflectance index (PRI) measured from the first fully expanded leaf blade. **P* < 0.05, ***P* < 0.001 (two-tailed Student's *t* test, comparing plants with and without PDMA treatment; *n* = 9, biological replicates). **c** Expression of the iron deficiency-marker gene *BdlRO2.1* and the iron overload-marker gene *BdFerritin* in roots. Plants were grown with 2.5 mg Fe L⁻¹ non-chelated iron ± PDMA (3, 30, 150, or 300 μM) or Fe-EDTA under HC for 3 weeks. **P* < 0.05, ***P* < 0.001 (two-tailed Student's *t* test,

comparing plants with PDMA treatment at various levels to those without PDMA; *n* = 3, biological replicates). **d** High-temperature treatment increases susceptibility to iron overload. Plants were grown under NC or HC with Fe-EDTA at a normal (45 μM, 2.5 mg Fe L⁻¹) or 100-fold higher concentration (4.5 mM, 250 mg Fe L⁻¹) for 2 weeks. H₂O₂ accumulation was detected in younger leaves using 3,3'-diaminobenzidine staining. Scale bars, 5 cm. **e** Expression of iron overload-marker gene *BdFerritin* in the first fully expanded leaves grown under NC or HC with chelated iron at normal (x1, 45 μM) or 100-fold higher concentration (x100, 4.5 mM) for 1 week. **P* < 0.05 (two-tailed Student's *t* test, comparing plants grown under normal and higher iron concentrations; *n* = 6, biological replicates). Data are means ± SEM. Exact *P* values for significant differences are shown on each graph. Source data are provided as a Source Data file.

homeostasis through chelation-based Fe uptake is crucial for enhancing resilience to prolonged high-temperature stress in the cool-season grasses wheat and *B. distachyon*. Our QTL analysis using *B. distachyon* identified a genomic region potentially involved in

mitigating prolonged high-temperature stress. This region contains the phyto siderophore efflux transporter *BdTOM1*, which is transcriptionally responsive to heat (Figs. 2 and 3). In fact, the high-temperature-tolerant accession Bd21-3 secreted higher levels of the

phytosiderophore DMA into the rhizosphere under HC than did the high-temperature-sensitive accession Bd21 (Fig. 2j). This suggests that Bd21-3 has a beneficial trait that allows it to recover from iron-deficiency stress under high temperatures. We further showed that the application of PDMA, a synthetic mugineic acid analog, can alleviate Fe-deficiency symptoms and restore biomass production under prolonged HC (Fig. 5). Nevertheless, when grown at high temperatures combined with Fe overload, plants accumulated more hydrogen peroxide (H_2O_2) and suffered greater cellular damage (Fig. 6). This Fe-overload-induced phenomenon (Fig. 6d and Supplementary Fig. 13d) is caused by the Fenton reaction, where excess free Fe reacts with H_2O_2 to generate highly reactive forms of ROS such as hydroxyl radicals ($\cdot\text{OH}$)³⁷. These findings suggest that the combination of excessive Fe and high temperature may lead to the production of more ROS, resulting in potentially deadly oxidative damage.

Unlike under Fe-excess conditions, HC caused yellowing of emerging leaves and suppressed plant growth under Fe deficiency, but these symptoms were not extreme and did not lead to seedling death, and they were reversible when plants were returned to NC (Supplementary Fig. 2). To cope with Fe deficiency, plants induce secretion of DMA that promotes Fe uptake, leading to an improvement of the Fe-deficiency state under prolonged high-temperature stress (Supplementary Fig. 14). When Fe deficiency is alleviated, the expression of iron-deficiency-related genes is rapidly switched off, suppressing DMA secretion, suggesting that the Fe-deficiency response can be mitigated without causing the detrimental effects of Fe overload. This finding suggests that reversible and temporary Fe deficiency can be beneficial, as it helps prevent the generation of ROS caused by excess Fe under high temperatures.

Under HC, leaf damage was less pronounced in seedlings treated with the chelated Fe form Fe-EDTA than in those treated with the non-chelated Fe form $\text{Fe}_2(\text{SO}_4)_3$, while PDMA treatment was more effective in promoting growth recovery (Fig. 6a–c, Supplementary Fig. 13a, b). Fe(III)-PDMA is a highly bioavailable form of Fe for uptake by transporters of the Yellow Stripe (YSL) and YSL-like family in graminaceous plants³⁸, and its application is more effective than Fe(III)-EDTA in improving Fe chlorosis in rice and maize (*Zea mays*)³⁹. The benefit of the synthetic phytosiderophore PDMA and natural phytosiderophores such as DMA can be attributed to their relatively short lifespan of ~2 weeks^{39,40}. This characteristic allows for the temporary enhancement of Fe uptake to a level sufficient to counteract Fe deficiency while preventing the detrimental effects of Fe overload under continuous HC.

Our findings suggest that the variation in resilience under prolonged heat stress among *B. distachyon* accessions stems from differences in Fe acquisition, as illustrated by the distinct patterns of induction of mugineic acid biosynthesis genes and DMA secretion (Figs. 2j and 3a, Supplementary Fig. 7a). Although *BdTOM1* emerged as a candidate gene associated with these differences based on our QTL analysis (Fig. 2) and subsequent analyses (Figs. 3 and 4, Supplementary Figs. 9, 10), whether the SNPs in *BdTOM1* affect the transport activity of its encoded proteins under HC remains unclear. For example, heat may directly affect or modulate *BdTOM1* transport activity through interactions with the lipids in the surrounding plasma membrane. The plasma membrane, in which TOM1 likely resides, is the primary site for sensing and transducing environmental signals, influencing aspects of cellular function related to membrane stability, ion transport, and stress acclimation⁴¹. Under HC, maintaining membrane stability is essential, as heat stress can disrupt the lipid bilayer, increasing permeability and potentially causing cellular damage. As a mitigation mechanism, plants maintain membrane fluidity and integrity by adjusting the levels of saturated fatty acids^{42,43}. Heat stress can also alter the distribution and/or activity of proteins at the plasma membrane. For instance, heat-induced activation of calcium channels at the plasma membrane can trigger temperature-signaling pathways⁴⁴, and

transcription factors like OsNTL3 relocate from the plasma membrane to the nucleus in response to heat⁴⁵. Future studies using transgenic approaches will help to further test the direct role of *BdTOM1* in heat tolerance.

In recent studies, liquid–liquid phase separation (LLPS) was shown to play a key role in environmental sensing by regulating protein–protein interactions^{46–48}. For example, TWA1, which undergoes structural changes under heat stress, accumulates in the nucleus via LLPS and interacts with transcription factors to promote the expression of heat-stress-responsive genes in *Arabidopsis*²². These mechanisms could potentially involve Fe homeostasis indirectly, but their precise role in heat-signaling pathways requires further investigation. In *B. distachyon*, Fe deficiency under HC did not alter the expression levels of *HSF* or *HSP* genes, encoding key regulators of the heat-shock response (Supplementary Fig. 7b). This result suggests that Fe deficiency is not directly involved in the early heat-shock response but rather acts downstream of it. Thus, heat-induced alterations in plasma membrane structure and function may affect the activity of plasma membrane-localized Fe transporters, such as the Fe^{2+} transporter IRON-REGULATED TRANSPORTER 1 (IRT1) and the Fe^{3+} -chelate reductases FERRIC REDUCTION OXIDASES (FROs), leading to altered Fe uptake and distribution, which may induce Fe deficiency symptoms under prolonged HC. Thus, when investigating the effect of *BdTOM1* haplotypes on mugineic acid secretion under prolonged HC, it is important to consider the characteristics of the plasma membrane, including changes in lipid composition, distribution, and the activities of related proteins.

Moreover, high-temperature environments disrupt ion uptake, which is critical for plant nutrition and growth^{49,50}. Our results show that Fe levels in leaves are lower under HC than under NC, while Mg and Mn levels are higher (Fig. 1f). Other heavy metals interfere with Fe homeostasis⁵¹. IRT1 and YSLs, which transport Fe and other heavy metals, may compete for the uptake of several heavy metals in roots, further exacerbating these imbalances⁵². Altered metal ion homeostasis, particularly an imbalance between Fe and other metals, can disrupt antioxidant enzyme functions, leading to ROS accumulation and intensified oxidative stress, ultimately causing oxidative damage to plant cells. Further analysis of metal ion homeostasis and its impact on antioxidant defense mechanisms in response to heat stress could provide a deeper understanding of Fe uptake and distribution in plant heat-tolerance mechanisms.

Cool-season cereals, including wheat and its relatives, are particularly vulnerable to rising global temperatures, posing a significant challenge to their cultivation in key agricultural regions. The Intergovernmental Panel on Climate Change (IPCC, 2023; <https://www.ipcc.ch/report/ar6/syr/resources/how-to-cite-this-report/>) projects a global mean temperature increase of 1.0–5.7 °C by the end of the 21st century, which is expected to result in more frequent and intense heat waves⁵³. For example, the interior plains of the North American Midwest, a global breadbasket, are projected to experience mean summer temperatures rising to 33 °C by 2100, and the land area suitable for wheat cultivation is projected to decrease by 10.9% ($\pm 24.2\%$) by 2100 under the moderate–high RCP6.0 emissions scenario⁵⁴. Wheat typically grows optimally at 18–24 °C⁵⁵, and *Brachypodium* species are adapted to temperate climates across the Mediterranean and the Indian subcontinent^{56,57}. Therefore, when grown under daytime temperatures of 35 °C, the growth of *Brachypodium* and wheat is markedly suppressed^{58,59}.

We examined the distribution of the two *BdTOM1* haplotypes among *B. distachyon* accessions collected from Turkey (Fig. 4b) but observed no clear geographical differences between them under current environmental conditions. However, our phenotypic analysis under temperature stress unveiled the potential properties of this variation. Conducting stress phenotyping under future climate scenarios reveals the potential resilience of plants to extreme

environmental conditions not yet encountered under current climate conditions. Applying this strategy to major crops and their close relatives or wild species could facilitate the development of mitigation strategies that enhance crop resilience and productivity. This approach offers a proactive means of safeguarding agricultural sustainability and food security against climate change.

Methods

Plant materials

The wheat (*Triticum aestivum*) cultivar ‘Fielder’ (KT020-061) was obtained from the National Bioresource Project (NBRP Komugi). *Brachypodium distachyon* accessions were originally obtained from Dr. David F. Garvin, Department of Agronomy and Plant Genetics, University of Minnesota, Minneapolis, MN, USA. F₉ generation recombinant inbred lines (RILs) were derived from a cross between *B. distachyon* accessions Bd21-3 (female) and Bd21 (male).

Plant growth conditions and prolonged high-temperature treatment

Seeds of wheat (Fielder) and the *B. distachyon* accessions were sown on two sheets of filter paper soaked in 7.5 ml of MilliQ water in a 9-cm (diameter) plastic Petri dish and incubated at 4 °C in the dark for several days. The seeds were then germinated in a growth chamber (BioTRON, NK Systems) at 25 °C under a 16-h-light/8-h-dark photoperiod, with a light intensity of 100–120 $\mu\text{mol m}^{-2} \text{s}^{-1}$. The relative humidity was maintained at 45–65%.

In the hydroponics system, the roots of wheat and *B. distachyon* seedlings were inserted through small holes in a foam board floating on the surface of half-strength Hoagland hydroponic solution in a plastic container. The seedlings were cultivated hydroponically under controlled conditions at 22–25 °C under the same photoperiod and light intensity as for seed germination. Half-strength Hoagland solution contained 2.5 mM KNO₃, 2.5 mM Ca (NO₃)₂, 1 mM MgSO₄, 0.5 mM KH₂PO₄, 1 mM K₂SO₄, 45 μM Fe(III)-EDTA (2.5 mg Fe L⁻¹), 23 μM H₃BO₃, 4.5 μM MnCl₂·4H₂O, 0.38 μM ZnSO₄·7H₂O, 0.16 μM CuSO₄·5H₂O, and 52 nM Na₂MoO₄·2H₂O, with the pH adjusted to pH 5.5–6.0. When the second leaf had partially emerged from wheat seedlings at the one-leaf stage or the third leaf had partially emerged from *B. distachyon* seedlings at the two-leaf stage, the roots of seedlings were rinsed with deionized water and transferred to a plastic container containing fresh half-strength Hoagland solution (adjusted to pH 5.5–6.0) supplemented with non-chelated iron provided as Fe₂(SO₄)₃ (corresponding to 2.5 mg Fe L⁻¹), in place of Fe(III)-EDTA. The plants were grown in the same growth chamber under normal-temperature conditions (NC, 22–25 °C) or high-temperature conditions (HC, 32–35 °C) under a 16-h-light/8-h-dark photoperiod, with a light intensity of 100–120 $\mu\text{mol m}^{-2} \text{s}^{-1}$, for several weeks. For gene expression analysis under iron-free conditions, *B. distachyon* seedlings were cultivated in iron-free, half-strength Hoagland hydroponic solution.

In the phenolic resin foam system, *B. distachyon* seeds were sown directly into artificial phenolic resin foam (oasis H1 block, Nisso Green Co., Ltd.) soaked in deionized water, incubated at 4 °C in the dark for several days, and cultivated in half-strength Hoagland hydroponic solution under NC and a 16-h-light/8-h-dark photoperiod with a light intensity of 100–120 $\mu\text{mol m}^{-2} \text{s}^{-1}$. When the third leaf had partially emerged from seedlings at the two-leaf stage, the blocks with seedlings were rinsed with deionized water, and the seedlings were transferred to a plastic container containing fresh half-strength Hoagland hydroponic solution with non-chelated iron [Fe₂(SO₄)₃] and grown in a growth chamber under NC or HC under a 16-h-light/8-h-dark photoperiod, with a light intensity of 100–120 $\mu\text{mol m}^{-2} \text{s}^{-1}$, for 4 weeks.

In the soil-based system, germinated wheat and *B. distachyon* seedlings were transferred to plastic pots containing a 1:1 (w/w) mixture of autoclaved Sakata Supermix-A (Sakata Seed Co. Ltd., Japan) and

vermiculite (Fukushima Vermi Co. Ltd., Japan), soaked in half-strength Hoagland hydroponic solution and grown under controlled conditions under a 16-h-light/8-h-dark photoperiod at a light intensity of 100–120 $\mu\text{mol m}^{-2} \text{s}^{-1}$. When the third leaf partially emerged from *B. distachyon* seedlings at the two-leaf stage, the seedlings were transferred to NC or HC and grown for 25 days under a 16-h light/8-h dark photoperiod.

Measurements of plant parameters

A portable handheld spectroradiometer (PolyPen RP410, Photon Systems Instruments-PSI, Czech Republic) was used to measure leaf spectral reflectance. Chlorophyll fluorescence was measured using a Junior-PAM chlorophyll fluorometer (Heinz Walz GmbH, Germany). The middle of each fully expanded Fielder or *B. distachyon* leaf blade was measured according to the manufacturer's instructions.

Element profiling of wheat cultivar ‘Fielder’

The top two leaves of wheat seedlings after 2 weeks of growth under NC or HC were dried at 55 °C for 3 days. The dried samples were digested using 60% (w/v) HNO₃. The concentrations of various mineral elements in the resulting solutions were determined using inductively coupled plasma mass spectrometry (NexION 350S, PerkinElmer, USA). The isotopes ²³Na, ²⁴Mg, ³⁹K, ⁴⁴Ca, ⁵⁵Mn, and ⁵⁷Fe were measured.

QTL analysis and analysis of fresh weight in 153 *B. distachyon* accessions

An F₂ population derived from a cross between *B. distachyon* accessions Bd21-3 (as the female) and Bd21 (as the male), comprising 758 individuals, was used for QTL analysis. A set of 418 genome-wide amplicon-seq markers was designed based on the single nucleotide polymorphisms (SNPs) originally identified by mapping whole-genome sequence reads from Bd21-3 onto the Bd21 reference genome (Bdistachyon_192_v1.2). Another F₂ population, derived from a cross between *B. distachyon* accessions Koz4 (as female) and Bd21 (as male), comprising 175 individuals, was included in the QTL analysis. A set of 443 genome-wide amplicon-seq markers was designed based on the SNPs between the Koz4 and Bd21 genomes. These markers were used for genotyping via amplicon sequencing to acquire polymorphic data. Amplicon-seq and SNP calling were conducted according to the multiplex PCR targeted amplicon sequencing (MTA-seq) method⁶⁰.

To measure fresh weight, seedlings from the F₂ individuals, RILs (see below), and 153 *B. distachyon* accessions were transferred to pots containing autoclaved soil (Pro-Mix Mycorrhizae, Premier Tech, Canada) and grown under controlled conditions under a 16-h-light/8-h-dark photoperiod and a light intensity of 100–120 $\mu\text{mol m}^{-2} \text{s}^{-1}$. When the third leaf partially emerged from *B. distachyon* seedlings at the two-leaf stage, the seedlings were transferred to NC or HC and grown for 25 days under a 16-h-light/8-h-dark photoperiod. The fresh weight of each shoot was then measured. For the *B. distachyon* accessions, the difference in fresh weight between accessions harboring the Bd21-type nonsynonymous SNPs and the Bd21-3-type nonsynonymous SNPs at *BdTOM1* was determined (Supplementary Data 2).

QTL analysis was performed using rQTL software, which initially identified a QTL on chromosome 4. To refine this QTL region, 371 SNP markers were strategically placed across the QTL region, and genotyping was conducted via amplicon-seq to enrich the polymorphic dataset in the Bd21-3 × Bd21 F₂ population. Moreover, a series of RILs was developed up to the F₉ generation from a cross between Bd21-3 (as the female) and Bd21 (as the male) through self-pollination using the single-seed descent method. These lines were genotyped via amplicon-seq; RILs with crossovers within the QTL region identified from the QTL mapping described above were used for a detailed examination of the correlation between high-temperature tolerance and genotype.

RT-qPCR analysis

Total RNA was extracted from the roots and leaves of seedlings using a NucleoSpin RNA Plant Kit (Takara Bio, Japan). First-strand cDNA was synthesized using ReverTra Ace qPCR RT Master Mix with gDNA remover (TOYOBO, Japan). RT-qPCR analysis was performed using TB Green Fast qPCR Mix (Takara Bio) on a TaKaRa Thermal Cycler Dice Real-Time System III. Data were normalized based on the expression of *BdUbi4* (Bradi3g04730) or *TaActin* (TraesCS5B02G124100.1) as described⁶¹. The comparative $2\Delta\Delta CT$ method was used for the quantification of gene expression. The primers used in this study are listed in Supplementary Data 6.

RNA-seq analysis

Root samples from seedlings grown in charcoal- and ceramic-based pebble growth medium (Charcoba, Impact Japan) were used for RNA-seq. The roots of *B. distachyon* seedlings were inserted through small holes in the pebble Charcoba medium in a plastic pot filled with half-strength Hoagland hydroponic solution. The seedlings were cultivated under NC. When the fifth leaf was partially emerged from seedlings at the four-leaf stage, the pots containing seedlings were rinsed with deionized water, and the plants were transferred to a plastic container containing fresh half-strength Hoagland hydroponic solution with 2.5 mg Fe L⁻¹ of non-chelated iron [Fe₂(SO₄)₃] and cultivated under NC or HC for 1 day. For PDMA treatment, 30 μ M PDMA was dissolved in half-strength Hoagland solution containing 2.5 mg Fe L⁻¹ of non-chelated iron, and the pH of the solution was adjusted to pH 5.5.

Sequencing libraries for RNA-seq were prepared using a NEXT-FLEX Rapid Directional RNA-Seq Library Prep Kit v2 following the manufacturer's protocol (PerkinElmer, USA). Pooled and barcoded libraries were sequenced on a DNBSEQ-T7 instrument (BGI, China) as paired-end 100-bp reads. The raw RNA-seq reads were quality checked and trimmed using Trimmomatic (v0.39)⁶² with the following parameters: SLIDINGWINDOW:4:15, LEADING:20, TRAILING:20, and MI MINLEN:50. Salmon (v1.9.0)⁶³ was used to quantify transcript abundance. The reads were mapped to the *Brachypodium distachyon* Bd21 reference genome (version Bdistachyon_314.v3.1) from Phytozome. Differentially expressed genes (DEGs) between NC and HC samples were identified using the R package DESeq2 (1.30.1)⁶⁴. DEGs were defined as $|\log_2[\text{fold-change}]| > 1$, false discovery rate < 0.05 .

Phylogenetic analysis

The amino acid sequences of Poaceae TOM family members were obtained from Phytozome (<https://phytozome-next.jgi.doe.gov/>) and Ensembl Plants (<https://plants.ensembl.org/index.html>). A phylogenetic tree was reconstructed using MEGA X^{65,66} with the neighbor-joining method⁶⁷. The alignment was further optimized by manual inspection and curation. SEQBOOT was used for bootstrapping with 1000 replicates. All ambiguous positions were removed from each sequence pair (pairwise deletion option). Evolutionary distances were computed using the Jones–Taylor–Thornton (JTT) matrix-based method⁶⁸.

Gene cloning and plasmid construction

The Bd21 genome sequence was obtained from Phytozome (<http://www.phytozome.net/brachy.php>). To generate the *Bdtom1* and *Bdtom3* mutants via CRISPR/Cas9-mediated gene editing, overlapping fragments used to clone the single-guide RNA (sgRNA) into a BbsI-digested guide plasmid (*BdU6* promoter-based pU6-gRNA vector) were PCR amplified using mutagenic pUCgRNA primers, as detailed in Supplementary Data 6. Subsequently, the two sgRNA cassettes digested with PacI/Ascl or XhoI/Ascl were individually inserted into the PacI/Ascl-digested pCambia BdUBQ3pro:OsCas9 vector. The resulting plasmids were individually introduced into Bd21 via *Agrobacterium tumefaciens*-mediated transformation as described previously^{69,70}. The construct used to produce *BdTOM1*-overexpressing (*Bdtom1#1*

BdTOM1) plants was generated using the In-Fusion system. The *BdTOM1* cDNA driven by the *B. distachyon* Ubiquitin promoter⁷¹ was introduced into the *Bdtom1#1* mutant via *A. tumefaciens*-mediated transformation. To generate genomic complementation lines, the *Bdtom1#3* mutant was transformed with an 8.6-kb genomic fragment containing the *BdTOM1* allele (gBdTOM1) derived from either Bd21 or Bd21-3 (Bd4 Bd4:31485037 - Bd4:31493673) in the Bd21 genome, Phytozome v3.2. The genomic fragments were cloned into a BamHI/Sall-digested pCambia1380-based vector using the NEBuilder HiFi DNA Assembly kit (New England Biolabs, USA). Each resulting construct was introduced into *Bdtom1 #3* via *A. tumefaciens*-mediated transformation, and transformants were selected based on hygromycin resistance. The complementation lines were grown in a growth chamber under normal temperature conditions using half-strength Hoagland hydroponic solution containing non-chelated iron [Fe₂(SO₄)₃]. Five independent complementation lines for each accession exhibited similar rescue phenotypes, and two representative lines were used for the analysis.

PDMA treatment

PDMA (provided by Dr. Suzuki, Aichi Steel Corporation)⁴⁰ was dissolved in half-strength Hoagland solution with 2.5 mg Fe L⁻¹ of non-chelated iron [Fe₂(SO₄)₃], and the pH of the solution was adjusted to pH 5.5. The resulting PDMA solution was applied to the rhizosphere every 10 days.

Measurement of iron content in leaf samples

The shoots of seedlings were dried at 55 °C for several days, and the Fe content was measured in the top two leaves from each seedling. The Fe²⁺ and Fe³⁺ concentrations in the leaves were measured using a Metallo Assay Kit following the LS Nitroso-PSAP method (Metallogenics, Japan), as per the manufacturer's instructions.

Geographical data collection and visualization

Geographical coordinates (latitude and longitude) for the collection sites of each *B. distachyon* accession were extracted and visualized using the Python programming language (version 3.9.13) with Matplotlib (version 3.5.2) and Cartopy (version 0.18.0) libraries. Collection site coordinates were obtained from field surveys or previously recorded data. Details of sample collection for *B. distachyon* accessions from Turkey were obtained from Vogel et al.⁷² (Supplementary Data 3).

DMA content measurements

B. distachyon seedlings were grown in half-strength Hoagland hydroponic solution with 2.5 mg Fe L⁻¹ of non-chelated iron [Fe₂(SO₄)₃] under HC for 2 weeks under a 16-h-light/8-h-dark photoperiod. To measure DMA content, the roots of seedlings were rinsed with deionized water and transferred to new plastic containers containing deionized water. After 5 h of light exposure at a light intensity of 100–120 μ mol m⁻² s⁻¹, DMA extracted from the roots and secreted into the hydroponic water was analyzed using high-performance liquid chromatography⁷³. The rate of DMA secretion was calculated using the following formula: % [DMA secretion/ (DMA secretion + root DMA content)].

Detection of hydrogen peroxide by DAB staining

To detect hydrogen peroxide (H₂O₂), *B. distachyon* and wheat leaf samples were stained with 3,3'-diaminobenzidine (DAB)⁷⁴. Briefly, the top leaves of *B. distachyon* and wheat plants grown under NC or HC were collected and incubated in 0.1% (w/v) DAB and 0.1% (v/v) Tween-20 in 10 mM sodium phosphate buffer (pH 7.8) at room temperature for 20 h in the dark with gentle shaking. Chlorophyll was removed by incubating the leaves in bleaching solution (ethanol: acetic acid: glycerol, 3:1:1, v/v/v) in a boiling water bath for 15 min.

Reporting summary

Further information on research design is available in the Nature Portfolio Reporting Summary linked to this article.

Data availability

The RNA-seq and raw sequencing data generated in this study have been deposited in the NCBI database under accession code [PRJNA1151630](https://doi.org/10.6084/m9.figshare.29670149.v3). Source data are provided in this paper. Source data are provided with this paper.

Code availability

Custom scripts for R/QTL analysis, transcript quantification using Salmon, and data visualization with Matplotlib are available at Figshare [<https://doi.org/10.6084/m9.figshare.29670149.v3>].

References

- Asseng, S. et al. Rising temperatures reduce global wheat production. *Nat. Clim. Change* **5**, 143–147 (2015).
- Akter, N. Heat stress effects and management in wheat. A review. *Agron. Sustain. Dev.* **37**, 37 (2017).
- Zhao, C. et al. Temperature increase reduces global yields of major crops in four independent estimates. *Proc. Natl Acad. Sci. USA* **114**, 9326–9331 (2017).
- Shew, A. M., Tack, J. B., Nalley, L. L. & Chaminuka, P. Yield reduction under climate warming varies among wheat cultivars in South Africa. *Nat. Commun.* **11**, 4408 (2020).
- Zhang, T. Climate change may outpace current wheat breeding yield improvements in North America. *Nat. Commun.* **13**, 5591 (2022).
- Mathur, S., Agrawal, D. & Jajoo, A. Photosynthesis: response to high temperature stress. *J. Photochem. Photobiol. B* **137**, 116–126 (2014).
- Scafaro, A. P. et al. Responses of leaf respiration to heatwaves. *Plant Cell Environ.* **44**, 2090–2101 (2021).
- Moore, C. E. et al. The effect of increasing temperature on crop photosynthesis: from enzymes to ecosystems. *J. Exp. Bot.* **72**, 2822–2844 (2021).
- Niu, Y. & Xiang, Y. An overview of biomembrane functions in plant responses to high-temperature stress. *Front. Plant Sci.* **9**, 915 (2018).
- Guihur, A., Rebeaud, M. E. & Goloubinoff, P. How do plants feel the heat and survive?. *Trends Biochem. Sci.* **47**, 824–838 (2022).
- Kan, Y., Mu, X.-R., Gao, J., Lin, H.-X. & Lin, Y. The molecular basis of heat stress responses in plants. *Mol. Plant* **16**, 1612–1634 (2023).
- Huang, Y. et al. HSF1a modulates plant heat stress responses and alters the 3D chromatin organization of enhancer-promoter interactions. *Nat. Commun.* **14**, 469 (2023).
- Bakery, A. et al. Heat stress transcription factors as the central molecular rheostat to optimize plant survival and recovery from heat stress. *N. Phytol.* **244**, 51–64 (2024).
- Yadav, M. R. et al. Impacts, tolerance, adaptation, and mitigation of heat stress on wheat under changing climates. *Int. J. Mol. Sci.* **23**, 2838 (2022).
- Wahid, A., Gelani, S., Ashraf, M. & Foolad, M. R. Heat tolerance in plants: an overview. *Environ. Exp. Bot.* **61**, 199–223 (2007).
- Hasanuzzaman, M., Nahar, K., Alam, M. M., Roychowdhury, R. & Fujita, M. Physiological, biochemical, and molecular mechanisms of heat stress tolerance in plants. *Int. J. Mol. Sci.* **14**, 9643–9684 (2013).
- Bitá, C. E. & Gerats, T. Plant tolerance to high temperature in a changing environment: scientific fundamentals and production of heat stress-tolerant crops. *Front. Plant Sci.* **4**, 1–18 (2013).
- Zhao, J., Lu, Z., Wang, L. & Jin, B. Plant responses to heat stress: physiology, transcription, noncoding RNAs, and epigenetics. *Int. J. Mol. Sci.* **22**, 117 (2020).
- Bourgine, B. & Guihur, A. Heat shock signaling in land plants: from plasma membrane sensing to the transcription of small heat shock proteins. *Front. Plant Sci.* **12**, 710801 (2021).
- Yamaguchi, N. et al. H3K27me3 demethylases alter HSP22 and HSP17.6C expression in response to recurring heat in Arabidopsis. *Nat. Commun.* **12**, 3480 (2021).
- Li, Z. et al. The heat shock factor 20-HSF4-cellulose synthase A2 module regulates heat stress tolerance in maize. *Plant Cell* **36**, 2652–2667 (2024).
- Bohn, L. et al. The temperature sensor TWA1 is required for thermotolerance in Arabidopsis. *Nature* **629**, 1126–1132 (2024).
- Yoneyama, T. Iron delivery to the growing leaves associated with leaf chlorosis in mugineic acid family phytosiderophores-generating graminaceous crops. *Soil Sci. Plant Nutr.* **67**, 415–426 (2021).
- Rai, S., Singh, P. K., Mankotia, S., Swain, J. & Satbhai, S. B. Iron homeostasis in plants and its crosstalk with copper, zinc, and manganese. *Plant Stress* **1**, 100008 (2021).
- Kawakami, Y. & Bhullar, N. K. Potential implications of interactions between Fe and S on cereal Fe biofortification. *Int. J. Mol. Sci.* **21**, 2827 (2020).
- Montejano-Ramírez, V. & Valencia-Cantero, E. Cross-talk between iron deficiency response and defense establishment in plants. *Int. J. Mol. Sci.* **24**, 6236 (2023).
- Kobayashi, T. & Nishizawa, N. K. Iron uptake, translocation, and regulation in higher plants. *Annu. Rev. Plant Biol.* **63**, 131–152 (2012).
- Li, Q., Chen, L. & Yang, A. The molecular mechanisms underlying iron deficiency responses in rice. *Int. J. Mol. Sci.* **21**, 43 (2020).
- Nozoye, T. et al. Phytosiderophore efflux transporters are crucial for iron acquisition in graminaceous plants. *J. Biol. Chem.* **286**, 5446–5454 (2011).
- Curie, C. et al. Maize yellow stripe1 encodes a membrane protein directly involved in Fe(III) uptake. *Nature* **409**, 346–349 (2001).
- Schaaf, G. et al. ZmYS1 functions as a proton-coupled symporter for phytosiderophore- and nicotianamine-chelated metals. *J. Biol. Chem.* **279**, 9091–9096 (2004).
- Yordem, B. K. et al. Brachypodium distachyon as a new model system for understanding iron homeostasis in grasses: Phylogenetic and expression analysis of Yellow Stripe-Like (YSL) transporters. *Ann. Bot.* **108**, 821–833 (2011).
- Scholtz, K. B. G., Irigoyen, S., Catalan, P. & Mandadi, K. K. Brachypodium: a monocot grass model genus for plant biology. *Plant Cell* **30**, 1673–1694 (2018).
- De Bang, T. C., Husted, S., Laursen, K. H., Persson, D. P. & Schjoerring, J. K. The molecular-physiological functions of mineral macronutrients and their consequences for deficiency symptoms in plants. *N. Phytol.* **229**, 2446–2469 (2021).
- Ogo, Y. Isolation and characterization of IRO2, a novel iron-regulated bHLH transcription factor in graminaceous plants. *J. Exp. Bot.* **57**, 2867–2878 (2006).
- Kim, S.-H. et al. Characterization of a novel DWD protein that participates in heat stress response in Arabidopsis. *Mol. Cells* **37**, 833–840 (2014).
- Dixon, S. J. & Stockwell, B. R. The role of iron and reactive oxygen species in cell death. *Nat. Chem. Biol.* **10**, 9–17 (2014).
- Yamagata, A. et al. Uptake mechanism of iron-phytosiderophore from the soil based on the structure of yellow stripe transporter. *Nat. Commun.* **13**, 7180 (2022).
- Suzuki, M., Suzuki, Y., Hosoda, K., Namba, K. & Kobayashi, T. The phytosiderophore analogue proline-2'-deoxymugineic acid is more efficient than conventional chelators for improving iron nutrition in maize. *Soil Sci. Plant Nutr.* 1–12, <https://doi.org/10.1080/00380768.2024.2385401> (2024).
- Suzuki, M. et al. Development of a mugineic acid family phytosiderophore analog as an iron fertilizer. *Nat. Commun.* **12**, 1–13 (2021).
- Zhao, X., Shi, Y., Chen, L., Sheng, F. & Zhou, H. Secondary structure changes and thermal stability of plasma membrane proteins of wheat roots in heat stress. *Am. J. Plant Sci.* **02**, 816–822 (2011).

42. Tang, T., Liu, P., Zheng, G. & Li, W. Two phases of response to long-term moderate heat: variation in thermotolerance between *Arabidopsis thaliana* and its relative *Arabis paniculata*. *Phytochemistry* **122**, 81–90 (2016).
43. Larkindale, J. & Huang, B. Changes of lipid composition and saturation level in leaves and roots for heat-stressed and heat-acclimated creeping bentgrass (*Agrostis stolonifera*). *Environ. Exp. Bot.* **51**, 57–67 (2004).
44. Saidi, Y. et al. The heat shock response in moss plants is regulated by specific calcium-permeable channels in the plasma membrane. *Plant Cell Online* **21**, 2829–2843 (2009).
45. Liu, X. et al. A membrane-associated NAC transcription factor OsNLT3 is involved in thermotolerance in rice. *Plant Biotechnol. J.* **18**, 1317–1329 (2020).
46. Jung, J.-H. et al. A prion-like domain in ELF3 functions as a thermosensor in *Arabidopsis*. *Nature* **585**, 256–260 (2020).
47. Zhang, H., Lang, Z., Zhu, J.-K. & Wang, P. Tackling abiotic stress in plants: recent insights and trends. *Stress Biol.* **5**, 8 (2025).
48. Liu, Q., Liu, W., Niu, Y., Wang, T. & Dong, J. Liquid–liquid phase separation in plants: advances and perspectives from model species to crops. *Plant Commun.* **5**, 100663 (2024).
49. Mishra, S., Spaccarotella, K., Gido, J., Samanta, I. & Chowdhary, G. Effects of heat stress on plant–nutrient relations: an update on nutrient uptake, transport, and assimilation. *Int. J. Mol. Sci.* **24**, 15670 (2023).
50. Soares, J. C., Santos, C. S., Carvalho, S. M. P., Pintado, M. M. & Vasconcelos, M. W. Preserving the nutritional quality of crop plants under a changing climate: importance and strategies. *Plant Soil* **443**, 1–26 (2019).
51. Lešková, A., Giehi, R. F. H., Hartmann, A., Fargasová, A. & Von Wirén, N. Heavy metals induce iron deficiency responses at different hierarchic and regulatory levels. *Plant Physiol.* **174**, 1648–1668 (2017).
52. Vert, G. et al. IRT1, an *Arabidopsis* transporter essential for iron uptake from the soil and for plant growth. *Plant Cell* **14**, 1223–1233 (2002).
53. Jagadish, S. V. K., Way, D. A. & Sharkey, T. D. Plant heat stress: concepts directing future research. *Plant Cell Environ.* **44**, 1992–2005 (2021).
54. Lyon, C. et al. Climate change research and action must look beyond 2100. *Glob. Change Biol.* **28**, 349–361 (2022).
55. Elbashir, A. A. E., Gorafi, Y. S. A., Tahir, I. S. A., Kim, J.-S. & Tsujimoto, H. Wheat multiple synthetic derivatives: a new source for heat stress tolerance adaptive traits. *Breed. Sci.* **67**, 248–256 (2017).
56. Wilson, P. B. et al. Global diversity of the *Brachypodium* species complex as a resource for genome-wide association studies demonstrated for agronomic traits in response to climate. *Genetics* **211**, 317–331 (2019).
57. Garvin, D. F. et al. Development of genetic and genomic research resources for *Brachypodium distachyon*, a new model system for grass crop research. *Crop. Sci.* **48**, S-69–S-84 (2008).
58. Djanaguiraman, M., Narayanan, S., Erdayani, E. & Prasad, P. V. V. Effects of high temperature stress during anthesis and grain filling periods on photosynthesis, lipids and grain yield in wheat. *BMC Plant Biol.* **20**, 268 (2020).
59. Ludwig, E. et al. Natural variation in *Brachypodium distachyon* responses to combined abiotic stresses. *Plant J.* **117**, 1676–1701 (2024).
60. Onda, Y., Takahagi, K., Shimizu, M., Inoue, K. & Mochida, K. Multiplex PCR targeted amplicon sequencing (MTA-Seq): simple, flexible, and versatile SNP genotyping by highly multiplexed PCR amplicon sequencing. *Front. Plant Sci.* **9**, 201 (2018).
61. Song, L. et al. Reducing brassinosteroid signalling enhances grain yield in semi-dwarf wheat. *Nature* **617**, 118–124 (2023).
62. Bolger, A. M., Lohse, M. & Usadel, B. Trimmomatic: a flexible trimmer for Illumina sequence data. *Bioinformatics* **30**, 2114–2120 (2014).
63. Patro, R., Duggal, G., Love, M. I., Irizarry, R. A. & Kingsford, C. Salmon provides fast and bias-aware quantification of transcript expression. *Nat. Methods* **14**, 417–419 (2017).
64. Love, M. I., Huber, W. & Anders, S. Moderated estimation of fold change and dispersion for RNA-seq data with DESeq2. *Genome Biol.* **15**, 550 (2014).
65. Kumar, S., Stecher, G., Li, M., Niyaz, C. & Tamura, K. MEGA X: molecular evolutionary genetics analysis across computing platforms. *Mol. Biol. Evol.* **35**, 1547–1549 (2018).
66. Stecher, G., Tamura, K. & Kumar, S. Molecular evolutionary genetics analysis (MEGA) for macOS. *Mol. Biol. Evol.* **37**, 1237–1239 (2020).
67. Saitou, N. & Nei, M. The neighbor-joining method: a new method for reconstructing phylogenetic trees. *Mol. Biol. Evol.* **4**, 406–425 (1987).
68. Jones, D. T., Taylor, W. R. & Thornton, J. M. The rapid generation of mutation data matrices from protein sequences. *Bioinformatics* **8**, 275–282 (1992).
69. Alves, S. C. et al. A protocol for *Agrobacterium*-mediated transformation of *Brachypodium distachyon* community standard line Bd21. *Nat. Protoc.* **4**, 638–649 (2009).
70. Mikami, M., Toki, S. & Endo, M. Comparison of CRISPR/Cas9 expression constructs for efficient targeted mutagenesis in rice. *Plant Mol. Biol.* **88**, 561–572 (2015).
71. Kouzai, Y. et al. BdWRKY38 is required for the incompatible interaction of *Brachypodium distachyon* with the necrotrophic fungus *Rhizoctonia solani*. *Plant J.* **104**, 995–1008 (2020).
72. Vogel, J. P. et al. Development of SSR markers and analysis of diversity in Turkish populations of *Brachypodium distachyon*. *BMC Plant Biol.* **9**, 88 (2009).
73. Higuchi, K. et al. Nicotianamine synthase gene expression differs in barley and rice under Fe-deficient conditions. *Plant J.* **25**, 159–167 (2001).
74. Daudi, A. & O'Brien, J. Detection of hydrogen peroxide by DAB staining in *Arabidopsis* leaves. *Bio Protoc.* **2**, e263 (2012).

Acknowledgements

This work was partially supported by the Cabinet Office, Government of Japan, Moonshot Research and Development Program for Agriculture, Forestry, and Fisheries (funding agency: Bio-Oriented Technology Research Advancement Institution), grant no. JPJ009237 to K.M. and the Japan Society for the Promotion of Science Grand-in Aid for Young Scientists (B) grant no. 17K15214 to Y.O. We thank David F. Garvin for providing the *Brachypodium distachyon* seeds. We also thank Kosuke Namba at Tokushima University for the development of the PDMA. Finally, we thank Fumiko Kato, Toshie Kita, Tomoko Okachi, Etsuko Kitada, and Hiromi Ojima for preparing plant materials.

Author contributions

A.M., Y.O., R.M., M.K., N.T. and K.M. conceived and designed the study. A.M. and K.M. developed the study and wrote the manuscript. A.M., Y.O., M.Shimizu., Y.U.-Y., R.N., T.Nomura, and Y.K. performed physical experiments. Y.U.-Y., K.Toyama. and M.E. prepared the transgenic plants, and T.Nozyo and K.Tanoi performed identification and quantification of DMA and inorganic elements, respectively. M.Suzuki. provided PDMA. Y.O., M.Shimizu., and K.M. conducted genotyping and QTL analysis. A.K., K.T. and K.I. analyzed the genomic sequence data.

Competing interests

M.Suzuki is employed by the company Aichi Steel Corporation. R.M., M.K. and N.T., are employed by Kaneka Co. Ltd. Other authors don't claim competing interests.

Additional information

Supplementary information The online version contains supplementary material available at <https://doi.org/10.1038/s41467-025-63005-0>.

Correspondence and requests for materials should be addressed to Anzu Minami or Keiichi Mochida.

Peer review information *Nature Communications* thanks Stephane Mari, who co-reviewed with Alexandra LeskovaLi Lei and the other, anonymous, reviewer(s) for their contribution to the peer review of this work. A peer review file is available.

Reprints and permissions information is available at <http://www.nature.com/reprints>

Publisher's note Springer Nature remains neutral with regard to jurisdictional claims in published maps and institutional affiliations.

Open Access This article is licensed under a Creative Commons Attribution-NonCommercial-NoDerivatives 4.0 International License, which permits any non-commercial use, sharing, distribution and reproduction in any medium or format, as long as you give appropriate credit to the original author(s) and the source, provide a link to the Creative Commons licence, and indicate if you modified the licensed material. You do not have permission under this licence to share adapted material derived from this article or parts of it. The images or other third party material in this article are included in the article's Creative Commons licence, unless indicated otherwise in a credit line to the material. If material is not included in the article's Creative Commons licence and your intended use is not permitted by statutory regulation or exceeds the permitted use, you will need to obtain permission directly from the copyright holder. To view a copy of this licence, visit <http://creativecommons.org/licenses/by-nc-nd/4.0/>.

© The Author(s) 2025